frontiers | Frontiers in Nanotechnology

TYPE Original Research
PUBLISHED 29 August 2025
DOI 10.3389/fnano.2025.1623625

OPEN ACCESS

EDITED BY
Chella Santhosh,
K L University, India

REVIEWED BY
Yilin Sun,
Beijing Institute of Technology, China
S. R. Srither,
Southern University of Science and Technology, China

*CORRESPONDENCE
Manish Pratap Singh,
drmanu99@gmail.com

RECEIVED 06 May 2025
ACCEPTED 17 July 2025
PUBLISHED 29 August 2025

CITATION
Singh A, Kumar A, Chaurasiya N, Rani A, Gupta M, Yadav BC and Singh MP (2025) Highly sensitive and fast-responsive room-temperature LPG sensor based on hydrothermally synthesized $MoTe_2$. *Front. Nanotechnol.* 7:1623625. doi: 10.3389/fnano.2025.1623625

Highly sensitive and fast-responsive room-temperature LPG sensor based on hydrothermally synthesized $MoTe_2$

Ankit Singh[1], Avdhesh Kumar[1], Navin Chaurasiya[2], Alka Rani[3], Monu Gupta[3], B. C. Yadav[3] and Manish Pratap Singh[1]*

[1]Department of Physics, Ionic Liquid and Nano Materials Laboratory, Faculty of Engineering and Technology, V. B. S. Purvanchal University, Jaunpur, India, [2]Department of Mechanical Engineering, Faculty of Engineering and Technology, V. B. S. Purvanchal University, Jaunpur, India, [3]Department of Physics, Nanomaterials and Sensor Research Laboratory, Babasaheb Bhimrao Ambedkar University, Lucknow, India

In the current study, a highly efficient and affordable sensor for liquefied petroleum gas (LPG) that operates at ambient temperature was fabricated using a thin film through an easy and low-cost approach. To achieve this objective, $MoTe_2$ was synthesized using a hydrothermal method. The synthesized material was characterized through powder X-ray diffraction (PXRD), Raman spectroscopy, Fourier transform infrared (FTIR) spectroscopy, field-emission scanning electron microscopy (FE-SEM), and energy-dispersive X-ray spectroscopy (EDS). According to the results of PXRD and Raman spectroscopy, a pure phase of layered $MoTe_2$ with a hexagonal structure without any notable impurities was formed. The average crystallite size of the synthesized material is ~37 nm. Raman spectroscopy and FTIR analysis revealed the presence of Mo–Te vibrational modes. The surface morphology reveals thin, wrinkled sheets with a crumpled topology having flake-like structures. The coexistence of Mo and Te elements was confirmed using the EDS study. The optimized sample was used to prepare the thin film using a spin-coating process. The sensing properties of the $MoTe_2$-based thin film were investigated as a room-ambient sensor for various LPG concentrations below the lower explosive limit of 0.5–2.0 vol%. The best sensor responses were recorded at 2.0 vol% LPG, with a value of 137, and at 0.5 vol% LPG, with a value of 26. Moreover, a rapid response time of 8 s and a recovery time of 22 s were observed at 0.5 vol% of LPG. These rapid dynamics are attributed to the prompt interaction between LPG molecules and pre-adsorbed oxygen species on the film surface, enabling fast adsorption-desorption cycles at active sensing sites. The results highlight the potential of $MoTe_2$ thin films as effective and scalable candidates for ambient LPG detection.

KEYWORDS

LPG sensor, thin films, hydrothermal method, transition metal dichalcogenides, sensor performance

1 Introduction

Unintentional release of flammable gases, such as liquefied petroleum gas (LPG), continues to be a major risk to infrastructure and public safety. Fires, explosions, and fatalities have been reported frequently in residential, commercial, and industrial settings. These incidents, which continue to occur alarmingly frequently despite advancements in safety procedures, are frequently caused by corroded pipelines, faulty fittings, poor maintenance, or user negligence. Because of their low ignition energy, quick diffusion, and accumulation in confined spaces, even minor leaks have the potential to become life-threatening situations if they are not discovered in a timely manner. This reality emphasizes how urgently effective and dependable sensing technologies that can continuously monitor environments and provide early warnings in the event of a gas release are needed.

LPG is an exceptionally flammable gas composed primarily of propane (C_3H_8) (5%–10%) and butane (C_4H_{10}) (70%–80%), along with a small amount of other hydrocarbons (Chaurasiya et al., 2023). It is predominantly used as a source of fuel at domestic and industrial levels. Its high flammability and volatility make it essential to detect leaks promptly to prevent fire hazards and explosions. The lower explosive limit (LEL) of LPG components is ~2% by volume in air, and regulatory exposure limits set by OSHA and NIOSH mandate early detection at levels well below this threshold (Singh et al., 2021). Gas sensors are a resistive type of sensors that have emerged as a vital tool in LPG detection. These sensors operate using a mechanism where gas adsorption modulates the charge carrier density of the sensing material (n or p type), leading to measurable changes to the resistance, as shown in Table 1. The key performance parameters of any gas sensor are sensitivity, selectivity, response/recovery time, operating temperature, and long-term stability.

So far, a wide variety of materials (viz. metal oxides, carbon nanotubes, graphene, MXene, transition metal dichalcogenides, perovskites, and metal organic frameworks) have been explored for LPG sensing (Gautam et al., 2021; Xu et al., 2017; Island et al., 2017; Dai et al., 2016; Bharati et al., 2024; Tiwari et al., 2022; Tiwari et al., 2024). Metal-oxide semiconductors (SMOs) such as ZnO, TiO_2, SnO_2, NiO, Fe_2O_3, and WO_3 have been widely studied for their chemical stability, cost effectiveness, ease of fabrication, and high sensitivity. These SMOs have the same working mechanism as that of resistive type of sensors. For example, Choudhary et al. (2021) synthesized α-Fe_2O_3 and examined their LPG-sensing performance. The fabricated sensor exhibits a response and a recovery time of 52 s and 107 s, respectively, with a sensor response of 87% toward 10 ppm of LPG at 170°C. Shinde et al. (2024) reported the ZnO-based LPG sensor with a sensor response of 367 toward 50 ppm at 350°C, with a rapid response time of 10 s. However, these SMOs often face challenges, such as high operating temperatures, long recovery time, and low selectivity, limiting their use in portable or room-temperature applications.

To address these limitations, two-dimensional (2D) materials have gained attention for their high surface-to-volume ratio, tunable electronic properties, and low activation energy for gas adsorption. Graphene, MoS_2, and MXenes have been successfully deployed in sensors for gases such as NO_2, NH_3, and H_2, with improved sensitivity and faster kinetics. Nevertheless, in the context of LPG sensing, studies based on 2D materials remain scarce, with most investigations confined to metal oxide or sulfide-based systems. Within the 2D material family, transition metal tellurides (TMTs), particularly $MoTe_2$, have emerged as highly promising but underexplored candidates. $MoTe_2$ exists in both semiconducting 2H and metallic 1T′ phases, offering a unique ability to tailor surface reactivity and charge transport behavior (Zappa, 2017). $MoTe_2$ is a suitable material for gas sensing because the Te atoms are the most favorable site for the adsorption of O_2 molecules in $MoTe_2$. This is owing to the longer bond length (3.93 Å) of Te–O compared to the shorter bond length of Mo–O_2 (2.71 Å) in $MoTe_2$. This also explains the facile release of gas molecules from the surface of $MoTe_2$ and enhances the rate at which the system returns to its original state (Zhu et al., 2014). Furthermore, $MoTe_2$ shows a narrow energy bandgap (direct type) of approximately 1.5 eV for a single layer and an indirect energy bandgap of approximately 0.83 eV for bulk $MoTe_2$. This is smaller than the bandgaps of other TMDs (Zhou et al., 2015; Octon et al., 2016). Furthermore, the higher charge carrier density in $MoTe_2$ than in other TMDs, like $MoSe_2$ and WSe_2, results in increased sensitivity to gas molecules (Su et al., 2019; Varghese et al., 2015). These characteristics make it a suitable candidate for gas-sensing applications, demanding high sensitivity and rapid response, particularly under ambient conditions. For example, Yan et al. (2024) reported room-temperature NO_2 gas sensing based on MoS_2/MoO_3 heterojunctions. The sensor exhibits 18.9 sensor responses at 1 ppm, with a response time and a recovery time of 20 s and 30 s, respectively. Munusami et al. (2022) reported room-temperature LPG and H_2 gas-sensing performance of MoS_2/graphene. The sensor showed a sensor response of 12.2 at 1,000 ppm LPG, with a response time and a recovery time of 15 s and 22 s, respectively, compared to H_2 gas. Kodan et al. (2024) reported $MoSe_2$–WS_2 room-temperature NO_2 gas-sensing performance. The sensor gives a sensor response of 59.63% to 50 ppb concentration, with a response time and a recovery time of 68.90 and 65.68 s, respectively.

Recent studies have shown that $MoTe_2$-based devices, including field effect transistors (FETs), exhibit strong gas-sensing behavior toward

TABLE 1 Variation of resistance of a sensor with gas and type of materials.

Type of material	Type of gas	Sensor response	Change in resistance	Majority charge carrier
N-type SnO_2	Reducing for LPG	$S = \frac{R_a}{R_g}$	Decreased	Electron
N-type SnO_2	Oxidizing for NO_2	$S = \frac{R_g}{R_a}$	Increased	Electron
P-type $MoTe_2$	Reducing for LPG	$S = \frac{R_g}{R_a}$	Increased	Hole
P-type $MoTe_2$	Oxidizing for NO_2	$S = \frac{R_a}{R_g}$	Decreased	Hole

oxidizing and reducing gases (Feng et al., 2017a; Wu et al., 2018a; Wu et al., 2018b). There are also some reports which show that other $MoTe_2$-based devices such as Schottky diodes exhibit even a better response and recovery time (Feng et al., 2017b; Shackery et al., 2018). Density functional theory and first-principles calculations further support $MoTe_2$'s sensitivity to various gas molecules (Liu et al., 2022; Cao et al., 2021; Panigrahi et al., 2019; Szary et al., 2022; Zhu et al., 2020; Feng et al., 2017a; Liu et al., 2021). Recently, Huang et al. (2025) reported layered $MoTe_2$/ZnO heterojunction for a sensitive TEA sensor at room temperature (RT). The sensor displayed a response time and a recovery time of 147 s and 173 s, respectively, with a sensor response of 91.9% at 19°C. Wu et al. (2025) reported a theoretical calculation using the first-principles DFT calculation for developing a ZnO–$MoTe_2$-based gas sensor. The results showed better adsorption and recovery performance for C_2H_6 than for CO_2 and H_2. However, a comprehensive study on $MoTe_2$ for LPG detection has yet to be reported.

The present work addresses this gap by investigating the LPG-sensing behavior of hydrothermally synthesized p-type $MoTe_2$ thin films at room temperature. The sensor exhibits high response, fast response/recovery time, and excellent selectivity toward LPG, demonstrating the potential of $MoTe_2$ as an effective and robust material for next-generation gas sensors for the first time.

2 Experiment

2.1 Materials

Sodium molybdate dihydrate ($Na_2MoO_4{\cdot}2H_2O \geq 99\%$), hydrazine hydrate ($N_2H_4.H_2O$, 98%), absolute ethanol (C_2H_5OH, 99.8%) and Tellurium metal powder (Te, 99.9% and ~200 mesh) were purchased from Sisco Research Laboratory (SRL) India. All the chemicals were used as received.

2.2 Hydrothermal synthesis of $MoTe_2$

Two millimole of $Na_2MoO_4.2H_2O$ and four millimole of Te powder were added to 140 mL of deionized (DI) water and stirred for 10 min; after that, 10 mL of $N_2H_4.H_2O$ was added in the above mixture. The resulting mixture was stirred for half an hour. The stirred mixture was transferred into a stainless-steel autoclave having a Teflon-lined sleeve. The autoclave was transferred into an oven at a temperature of 200°C for a reaction time of 48 h. Once the reaction was complete, the autoclave was allowed to cool at room temperature. The obtained sample was rinsed with an abundant amount of DI water and ethanol, and subsequently dried for 12 h at a temperature of 60°C. The synthesis process of hydrothermally synthesized $MoTe_2$ is depicted in Figure 1.

2.3 Thin-film preparation of pristine $MoTe_2$

A photo-resist spin coater was used to prepare the thin film from the synthesized p-type $MoTe_2$ sample on a 2 × 1 cm^2 glass substrate. Initially, the glass substrate was cleaned via an ultrasonic cleaner using DI water and ethanol. DI water was used to dissolve the sample for the preparation of the dilute $MoTe_2$ solution. The diluted solution was subjected to sonication. The resulting solution was dropped on the clean glass substrate and placed on a spin coater for 60 s at 3,000 rpm, followed by drying of the coated glass substrate at

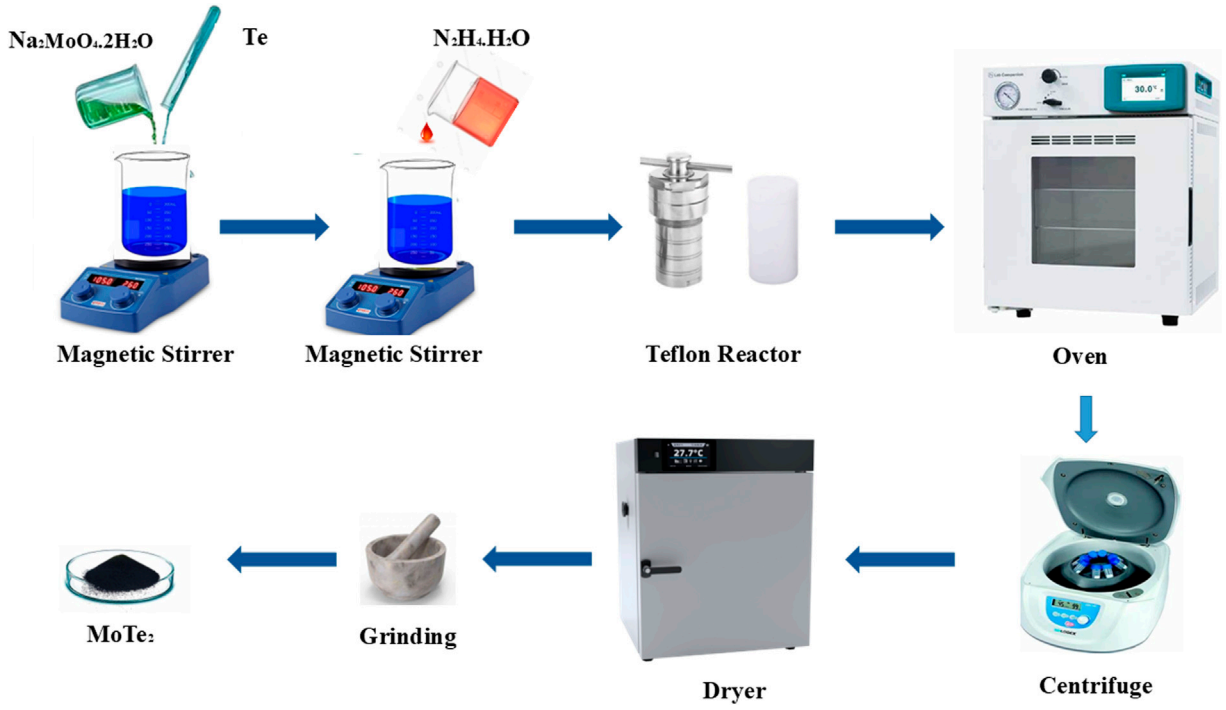

FIGURE 1
Illustration of hydrothermal synthesis of layered $MoTe_2$ nano-material.

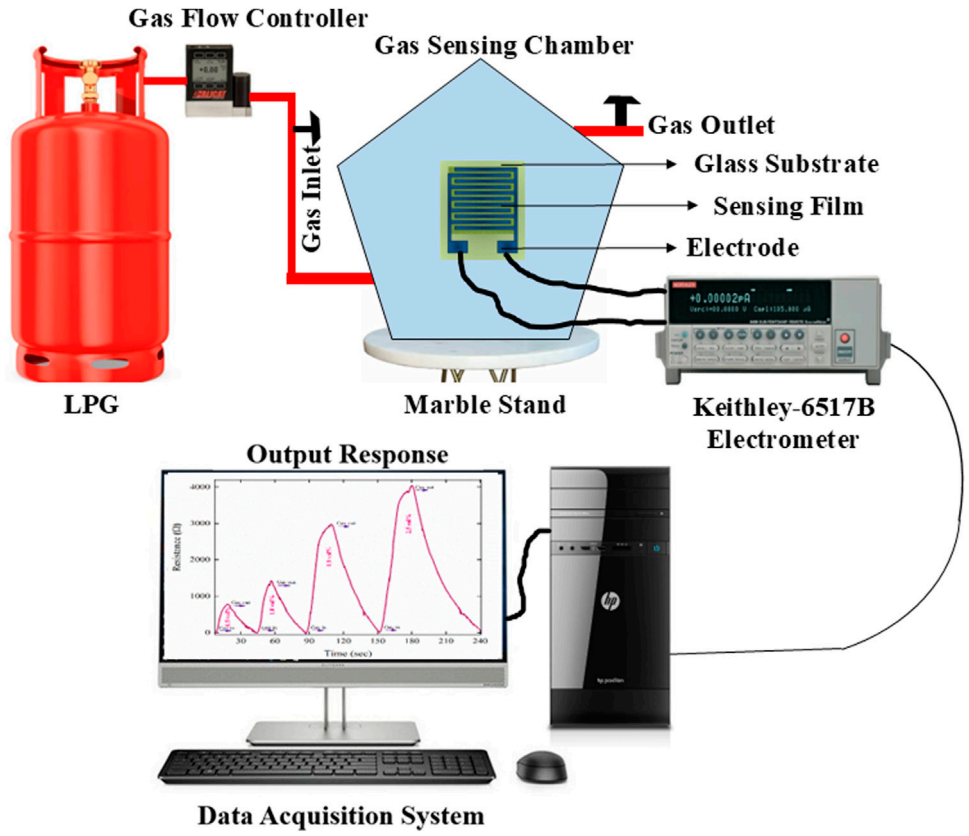

FIGURE 2
Diagram illustrating the LPG-sensing setup.

50°C for 5 minutes. To obtain the necessary thickness of the thin film, the same procedure was repeated.

2.4 Characterization

The hydrothermally synthesized $MoTe_2$ was characterized using powder X-ray diffraction (PXRD). The PXRD data from the hydrothermally synthesized samples were collected in the range of 20°–70° 2θ using a EMPYREAN diffractometer having Cu Kα radiation sources, with wave length λ = 1.5406 Å and operated at 40 kV. The morphology and elemental composition/mapping were examined using Nova Nano SEM 450 field emission scanning electron microscopy (FE-SEM) of USA, assembled with energy-dispersive electron X-ray spectroscopy (EDX, Team Pegasus Integrated EDS-EBSD with Octane Plus and Hikari Pro, EDX Inc.) operated at 15 kV. A Raman spectrometer (Renishaw in Via RE04) having 532 nm excitation wavelength with a resolution of 3 cm^{-1} was used to record the data. The FTIR spectra were collected using a Thermo Nicolet Avatar 370 spectrometer. The resolution in FTIR spectra was 4 cm^{-1}.

2.5 LPG-sensing setup

The experimental evaluation of the sensor's sensing capabilities was conducted by monitoring the fluctuation in electric current during exposure to LPG. A gas chamber constructed from borosilicate glass was designed specifically for detecting LPG gas. The chamber is equipped with inlet and outflow knobs for the purpose of inserting and removing LPG, respectively. The gas chamber consists of a concentration-measuring apparatus, in which the gas chamber was connected to a gas cylinder, along with a mass flow controller that quantified the gas admitted in vol.%. Furthermore, an outlet knob was designed to withdraw unadsorbed LPG. The contacts were made on the prepared thin film using silver paste. The sensing device was connected to a Keithley electrometer (model 6517B) manufactured by Tektronix, Beaverton, Oregon, USA. This electrometer was connected with a sensing device at one terminal and a computer system handling the measurement of electrical data, including current and resistance, at the other terminal, as shown in Figure 2.

3 Results and discussion

3.1 PXRD

PXRD is used to examine the purity of the synthesized phase and crystalline nature of the synthesized sample. The PXRD pattern of the synthesized sample is shown in Figure 3. The diffraction peaks for pristine $MoTe_2$ were observed at 2θ angles of 23.13°, 27.61°, 38.38°, 40.57°, 43.47°, 46.03°, 47.11°, 49.77°, 51.35°, 52.07°, 57.05°,

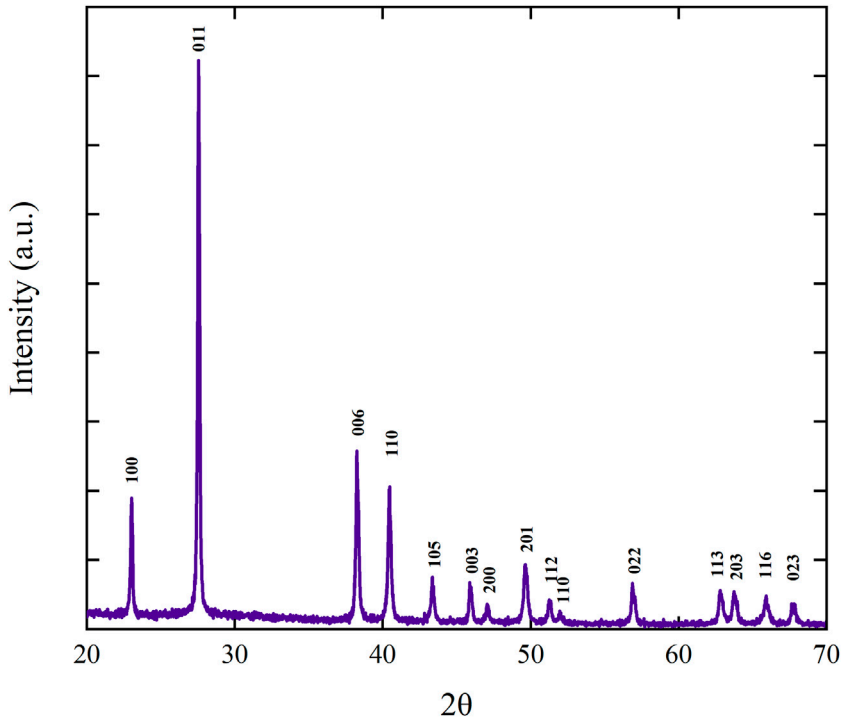

FIGURE 3
PXRD pattern of $MoTe_2$.

62.99^0, 63.83^0, 66.02^0, and 67.71^0 corresponding to the crystal planes (100), (011), (006), (110), (105), (003), (200), (201), (112), (110), (022), (113), (203), (116), and (023) of molybdenum ditelluride, respectively. All the observed diffraction peaks are well indexed. The PXRD pattern of the synthesized material ($MoTe_2$) is also matched well with JCPDS card no 01-073-1650 and 01-079-0736 (for Te) (Bhat and Nagaraja, 2019; Chen et al., 2022). The observed PXRD pattern does not contain any additional peaks associated with impurity phases or the monoclinic 1T′ polymorph. The absence of 1T′-specific reflections at ~ 14.2°, ~29.8°, and ~35.5°, along with the agreement between the observed diffraction pattern and standard reference data, support the formation of the semiconducting 2H–$MoTe_2$ structure. This outcome confirms the validity of the synthesis technique used in this investigation and is consistent with earlier reports on hydrothermally synthesized $MoTe_2$ (Chen et al., 2022; Bhat and Nagaraja, 2019). The Scherrer's equation was used to calculate the average crystallite size, as presented in Equation 1:

$$D_{hkl} = \frac{0.9\lambda}{\beta_{hkl} Cos\, \theta_{hkl}}. \quad (1)$$

Here, λ is the wavelength of X-ray in radians, θ_{hkl} is Bragg's angle of diffraction, and β_{hkl} is the full width at half maxima (FWHM) of the peaks (radians). The average size of the crystallite is found to be 37.14 nm. The percent crystallinity of synthesized nanostructured $MoTe_2$ is also calculated using the area of the crystalline peaks to the total area. The % crystallinity is found to be ~95%. This shows that synthesized nano $MoTe_2$ material has an excellent crystallinity. The excellent crystallinity of synthesized nano $MoTe_2$ results from a precisely regulated synthesis process using high-purity precursors, with the possibility of the presence of weaker Te rings in synthesized nano $MoTe_2$. The existence of feebler Te rings serves as a center of nucleation or substrates, facilitating the growth of $MoTe_2$.

3.2 FTIR spectroscopy

FTIR analysis offers important information regarding the functional groups and various types of chemical bonds present in the materials. The FTIR spectrum of synthesized $MoTe_2$ nano-material is used to analyze the vibrational bands of synthesized nano $MoTe_2$ in the frequency range between 4,000 and 500 cm^{-1}. The recorded FTIR spectrum of synthesized nano $MoTe_2$ is depicted in Figure 4. The FTIR spectrum of the synthesized nano $MoTe_2$ material show a vibrational band at 1,632 cm^{-1}. The band assigned to this is attributed to the bending mode of adsorbed water, whereas the wide band at 3,447–3,499 cm^{-1} is assigned to a O–H stretching mode of liquid or adsorbed water H–O–H (Shinde et al., 2021; Singh et al., 2017). Additionally, the vibrational band observed at 1,084 cm^{-1} is assigned to the stretching mode of metal oxide (M–Ox) bonds (Abdullah et al., 2023; Shirpay and Mohagheghi, 2020). The vibrational bands observed at a low wave number of 602 cm^{-1} and a vibrational peak at 735 cm^{-1} correspond to the vibrational mode of metal-telluride for nano $MoTe_2$ (Abdullah et al., 2023). The vibrational frequency at 1,435 cm^{-1} is corresponding to Te–O oxidation vibrational modes. The presence of characteristic vibrational modes of synthesized nano $MoTe_2$ validates the effective synthesis of the $MoTe_2$ material.

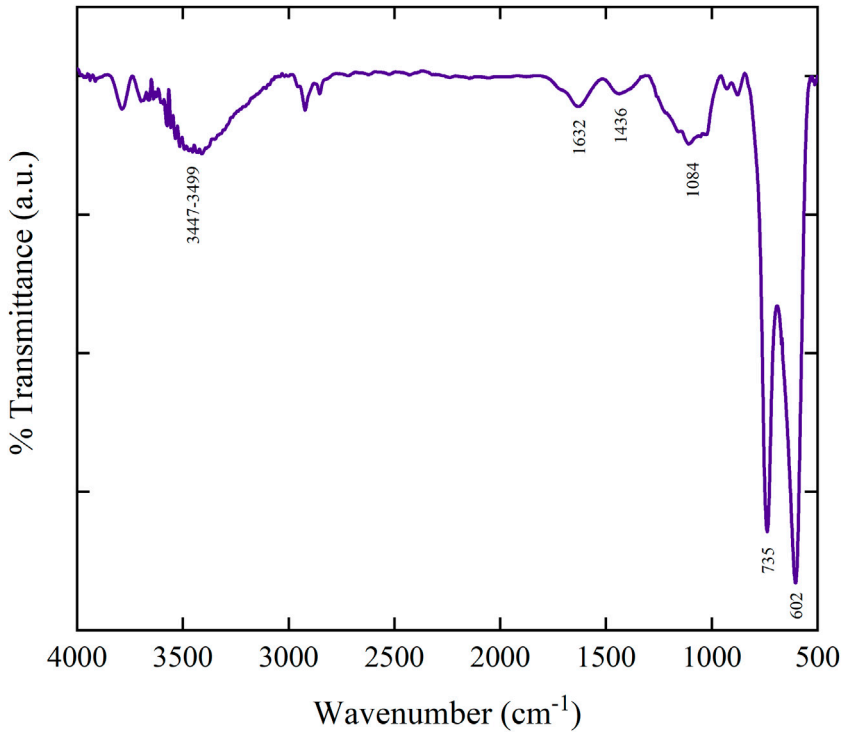

FIGURE 4
FTIR graph of synthesized $MoTe_2$.

3.3 Raman spectroscopy

Raman spectroscopy is a powerful method for investigating vibrational modes, detecting defects, and assessing structural phase purity. A LASER source of 532 nm was used to record the Raman spectrum of the $MoTe_2$ nano-crystalline material. Figure 5 presents the Raman spectrum of $MoTe_2$ recorded between 1,000 and 80 cm^{-1}. $MoTe_2$ exhibits all the Raman active modes in the investigated range. These three prominent modes of vibration correspond to the characteristic vibrational modes of $MoTe_2$. The vibrational mode at 224 cm^{-1} corresponds to the conspicuous in-plane E^1_{2g} mode of vibration. The E^1_{2g} peak signifies the in-plane vibration induced by two tellurium atoms in relation to a molybdenum atom (Grzeszczyk et al., 2016). The existence of this mode of vibration indicates the formation of the layered $MoTe_2$ structure. The vibrational mode at 175 cm^{-1} corresponds to the out-of-plane A_{1g} mode. The in-plane E_{1g} mode is observed at 118 cm^{-1}. The presence of the weaker A_{1g} mode also confirms few numbers of layers in the synthesized $MoTe_2$. All the observed vibrational modes of Raman corresponding to E^1_{2g}, A_{1g}, and E_{1g} modes are in good agreement with the 2H phase of $MoTe_2$. The absence of additional bands that typically arise in the monoclinic 1T′ phase—characterized by complex multiple structures due to the reduced symmetry—confirms that the synthesized sample is structurally consistent with the semiconducting 2H phase. These vibrational characteristics are in strong agreement with previously reported Raman profiles for hexagonal 2H–$MoTe_2$. This result is consistent with the PXRD analysis, confirming the formation of the pure 2H–$MoTe_2$ phase (Zhou et al., 2015; Guo et al., 2015; Lv et al., 2017).

3.4 FE-SEM

The morphology and structure of the $MoTe_2$ material were analyzed using FE-SEM. Figure 6a, b depicts the FE-SEM micro-images of $MoTe_2$ synthesized using the hydrothermal technique. Figure 6a shows a disordered and highly textured surface with prominent flake-like and platelet structures. These flakes appear randomly oriented and aggregated into loosely packed clusters, suggesting a layered morphology. The lateral dimensions of the flakes range from ~200 to 800 nm, with thicknesses consistent with few-layered to multilayered structures. Additionally, several elongated features are observed, which may indicate anisotropic growth behavior, possibly driven by the directional energy minimization along specific crystallographic planes during hydrothermal synthesis. Figure 6b shows thin, wrinkled sheets with a crumpled topology, consistent with exfoliated or few-layered 2D layers. These morphological features are indicative of weak van der Waals interactions between the layers, facilitating delamination and restacking. Notably, numerous ultrafine nanoparticles can be observed uniformly distributed on or near the $MoTe_2$ flakes. These particles are attributed to a nucleation center. This morphology is consistent with the crystallographic features identified in PXRD analysis. The diffraction peaks observed at 2θ values of 38.38°, 43.47°, 52.07°,

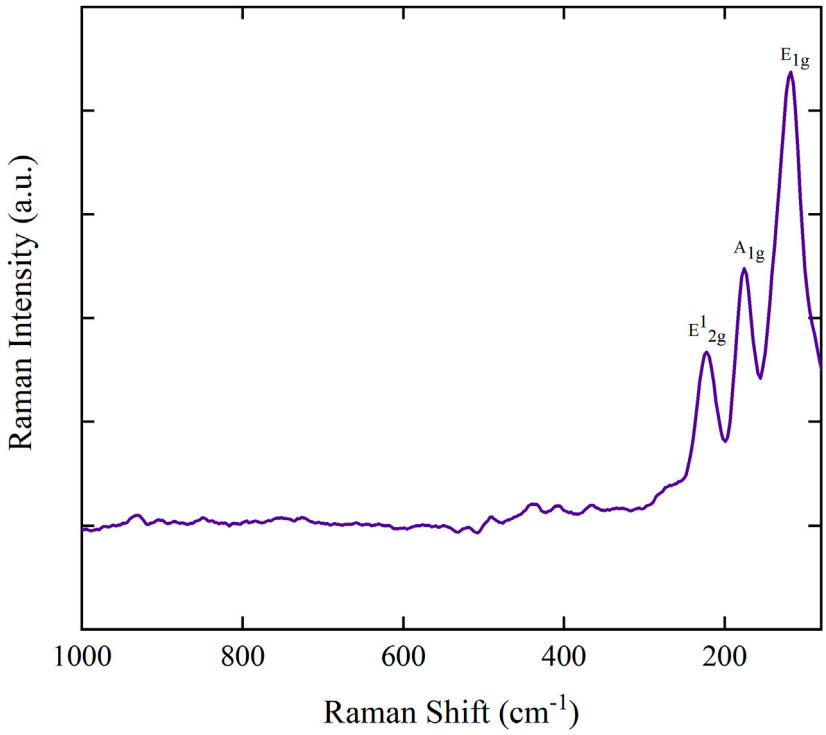

FIGURE 5
Raman spectra of synthesized layered $MoTe_2$ nano-material.

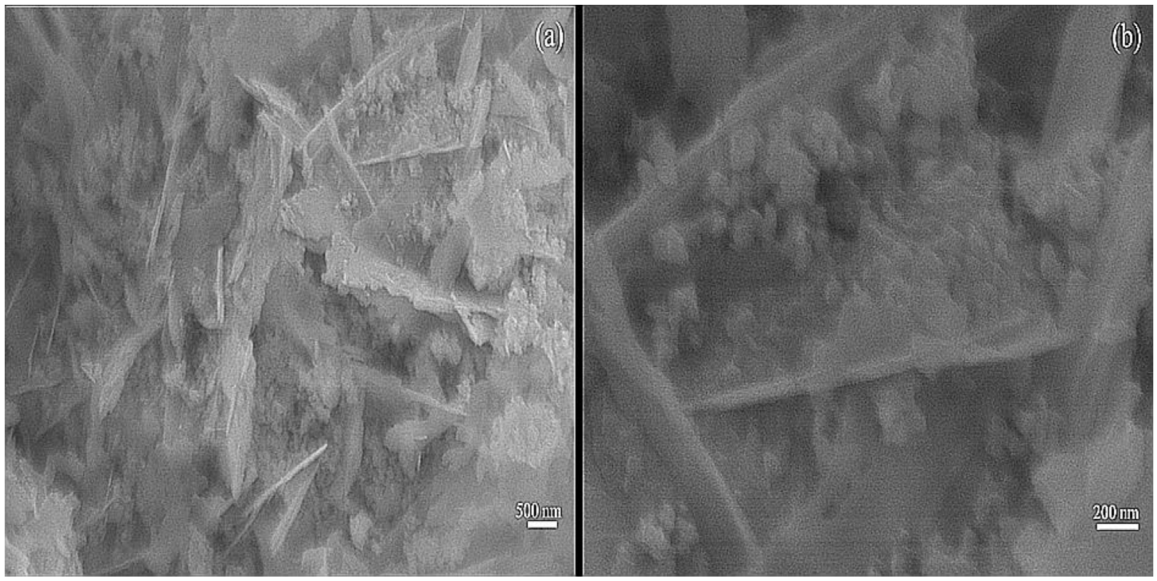

FIGURE 6
FE-SEM images of synthesized MoTe2 **(a)** lower magnification, **(b)** higher magnification.

63.83° and 66.02° correspond to the (006), (105), (110), (203) and (116) planes of hexagonal 2H–$MoTe_2$, respectively, confirming the formation of a layered structure. Raman observations also complemented these findings by revealing a few-layer configuration, which aligns with the thin-sheet morphology observed in the SEM. Together, the SEM, PXRD, and Raman results confirm that the synthesized $MoTe_2$ possesses a layered, few-sheet architecture, with high crystallinity and pure 2H symmetry, which is ideal for applications requiring efficient surface interaction and charge transport.

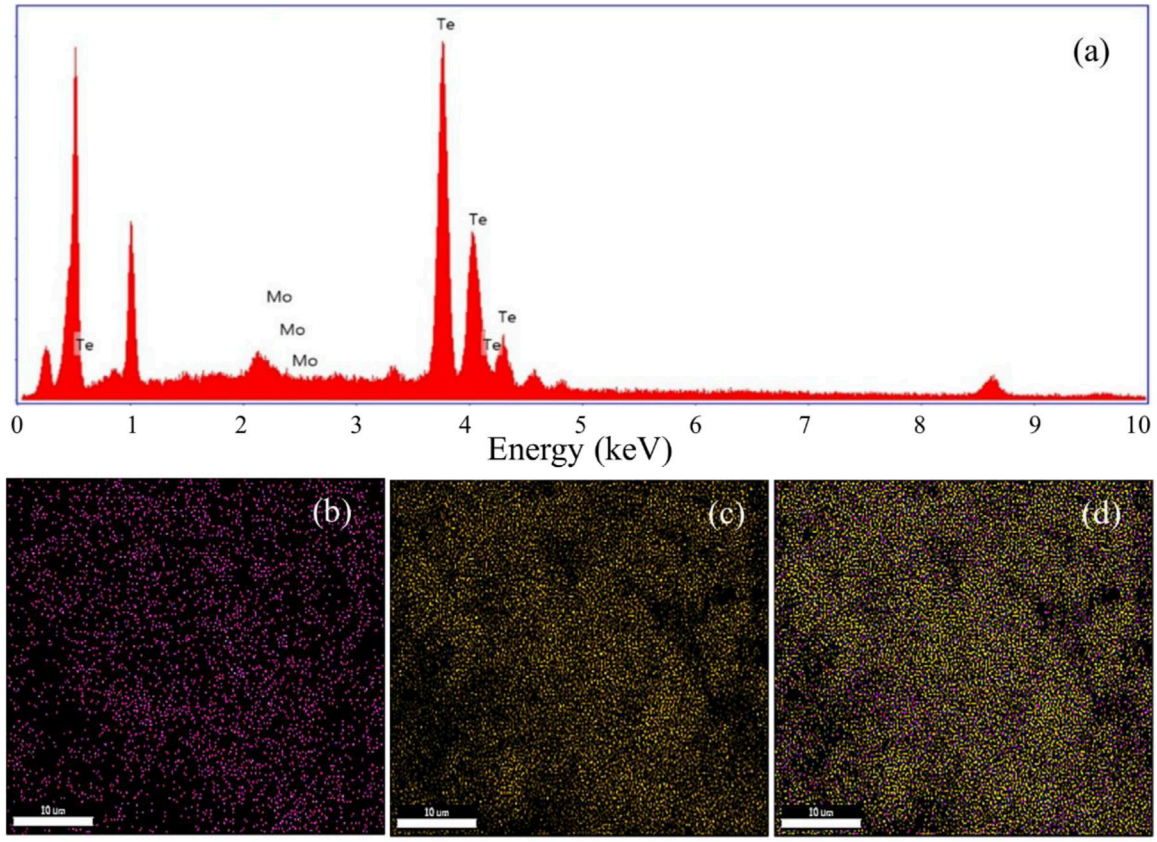

FIGURE 7
EDS spectra of synthesized $MoTe_2$. **(a)** Elemental mapping of Mo **(b)**, elemental mapping of Te **(c)**, and elemental mapping of $MoTe_2$ **(d)**.

Furthermore, the EDS analysis, as shown in Figure 7a, was conducted to determine the composition of the elements present in the synthesized $MoTe_2$ nano-material. The results confirm that the material primarily consists of two elements: molybdenum (Mo) and tellurium (Te). Figures 7b–d display the elemental distribution and color mapping of $MoTe_2$, revealing a uniform dispersion of Mo and Te throughout the sample. It is also worth noting that the color mapping indicates a Te-rich pattern, which aligns with the PXRD observation and is attributed to the presence of weaker Te rings (Bhat and Nagaraja, 2019).

4 LPG-sensing performance of the $MoTe_2$-sensing film

The LPG-sensing capabilities are assessed by investigating the change in electrical resistance of the prepared $MoTe_2$ thin-film sensor at 0.5–2.0 volume % of LPG concentration at an ambient temperature. Figure 8 illustrates the response and recovery properties of the $MoTe_2$-sensing film after exposure to a range of concentrations from 0.5 to 2.0 vol%, below the LEL value. First, the value of sensor's current is set fixed at a constant value in air, and then, the static resistance was observed in air. This is taken as R_a. Second, the thin film was exposed through LPG, and the change in resistance (R_g) was recorded. To check the all-inclusive sensor's parameters, such as response and recovery time, selectivity, and sensitivity, relevant tests were conducted. Figure 8 shows the response of the sensor at various concentrations of LPG. A strong correlation between the detection capabilities of the sensor and the gas concentration is shown by the fact that as the LPG concentration increases from 0.5 to 2.0 vol%., it is interesting to observe that the resistance of the sensing element increases with the LPG concentration. The sensor response of the prepared thin-film sensor is determined by the ratio of the measured resistance (when exposed to the target gas) to the resistance in the air. The response of the thin-film sensor at different concentrations of LPG was determined using Equation 2 (Verma et al., 2022; Singh et al., 2021) and presented in Figure 9a.

$$S.R = \frac{R_g}{R_a}, \tag{2}$$

where R_g is the resistance after LPG exposure and R_a is the resistance in the air. Figure 9a shows that the sensor response at a low concentration of LPG (0.5 vol%) is 26. In contrast, the largest sensor response was determined as 137 at 2.0 vol% LPG concentration. It is demonstrated that with the increase in the concentration of LPG, the sensor response increases linearly (Figure 9a), indicating that a smaller amount of the gas interacts with a smaller portion of the sensing film surface. However, when the LPG concentration increases, the area covered by the gas also increases proportionately; therefore, an increased surface contact is established between the LPG and the thin-film sensor, consequently

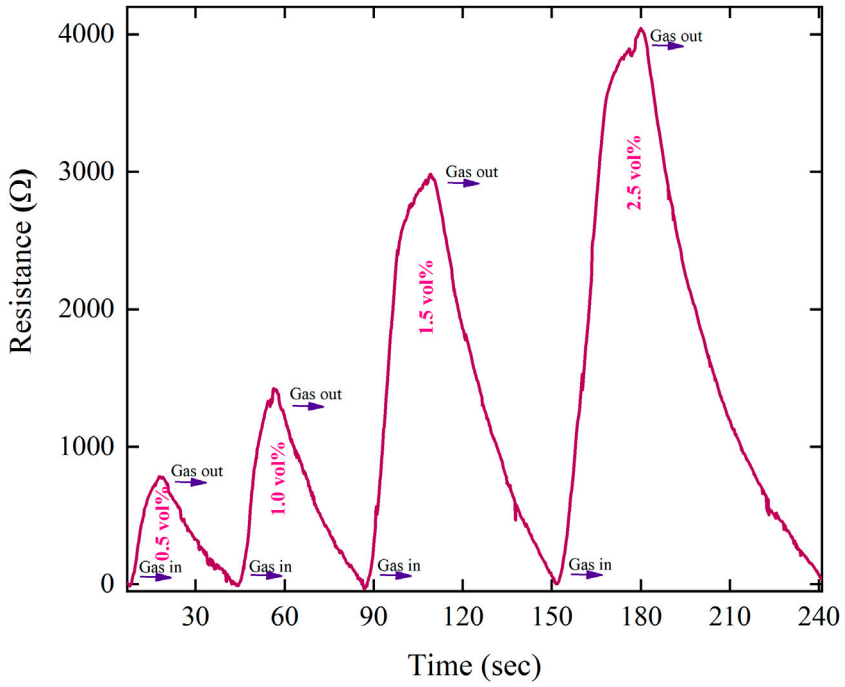

FIGURE 8
Response transient of the $MoTe_2$ thin film for varying LPG concentrations (0.5–2.0 vol%).

increasing the sensor response. The sensitivity of the LPG sensor is defined as the ratio of the change in the resistance to the change in the concentration (Verma et al., 2022).

$$S = \frac{\Delta R}{\Delta C} = \frac{\text{change in resistance}}{\text{change in concentration}}. \quad (3)$$

To find out the value of the sensitivity of the thin-film sensor, a linear regression analysis was carried out. The value of sensitivity is obtained from the slope of linear fitting of LPG vol% vs. sensor response. The evaluated value of sensitivity was 77 sensor response per vol%. Moreover, the R^2 factor value was 0.97, indicating that even the device operates well below the LEL. This sensitivity value and R^2 generally describe the reliability of the LPG sensor.

The fabricated $MoTe_2$ thin film has a faster response and recovery time for low-concentration gas than for high-concentration LPG. The determination of response and recovery time is derived using the characteristic graph (Figure 8). The response and recovery curves of the sensing film at different LPG concentrations are depicted in Figure 9b. The time of response of the sensing films was determined by measuring how long it takes for their resistance to change by 90% after exposure to LPG. Similarly, the time of recovery of the sensing films was determined by measuring how long it takes for their resistance to change by 90% and return to its initial value after the removal of the LPG. The characteristic curve of the sensor response for 0.5 vol% of LPG is presented in Figure 9c. An excellent sensor response and a recovery time of 8 and 22 s, respectively, were achieved for 0.5 vol% LPG. Table 2 shows the sensor response and time of response and recovery at different concentrations of LPG.

Repeatability is an essential sensor parameter that refers to the ability to consistently produce the similar result over a specific time interval for similar measurements. The recurrence graph for 1.5 vol % LPG using the $MoTe_2$ sensor film is shown in Figure 9d, which displays four consecutive cycles. Here, we found that the reported sensor yielded a result of 99.40%, with an error of only 0.6%. This is possibly due to the presence of moisture, which reduces the absorption capacity (Hu et al., 2012).

Selectivity is a sensor's ability to differentiate the gas of interest from other analyte gases. High selectivity indicates a stronger response of the sensor to the target gas than to other analyte gases. In this study, variety of gases are used to evaluate the $MoTe_2$-sensing film's selectivity using methanol (CH_3OH), LPG, ethanol (C_2H_5OH), acetone (CH_3COCH_3), and carbon dioxide (CO_2) for 0.5 vol% at room temperature, as illustrated in Figure 10a. The sensor responses to methanol, LPG, ethanol, acetone, and CO_2 are recorded as 12, 26, 10, 5, and 3, respectively. Additionally, the coefficient of selectivity (K) of all gases used in this study is evaluated from Equation 4:

$$K = \frac{S.R_{LPG}}{S.R_{Gas}}, \quad (4)$$

where $S.R_{LPG}$ and $S.R_{Gas}$ represent the sensor response for LPG and other gases, respectively. The thin film exhibited a selectivity coefficient of 2.16 for methanol, 2.6 for ethanol, 5.2 for acetone, and 8.6 for CO_2. A higher K-value indicates greater selectivity in LPG detection than in the detection of other gases used in this study. For example, a K-value of 2.16 for methanol describes that the response of the sensor toward LPG is 2.16 times greater than that of methanol. These results indicate that the $MoTe_2$-sensing film exhibits the highest selectivity coefficient toward LPG of all other analyte gases. The performance of the fabricated thin-film sensor based on the synthesized $MoTe_2$ nanomaterial is compared with the recently

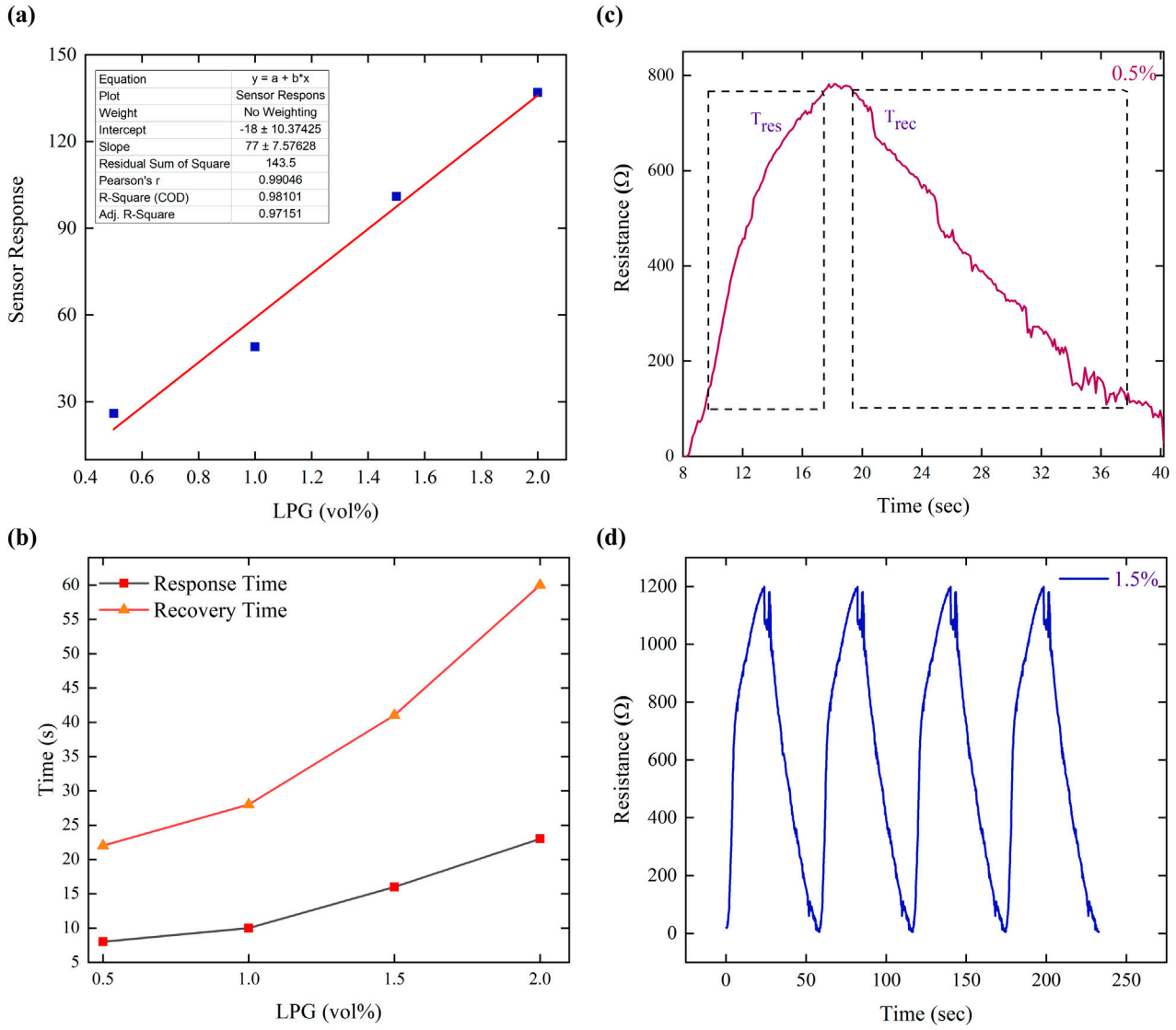

FIGURE 9
(a) LPG volume % vs. response of sensor of the $MoTe_2$ thin-film sensor. **(b)** LPG concentration-dependence time of response and time of recovery. **(c)** Sensing response curve at 0.5 volume % LPG. **(d)** Reproducibility for 1.5 volume % LPG.

TABLE 2 Sensor parameters for $MoTe_2$ at different concentrations of LPG.

LPG volume %	Temperature	Time of response (s)	Time of recovery (s)	Response of sensor
0.5	RT	8	22	26
1.0	RT	10	28	49
1.5	RT	16	41	101
2.0	RT	23	60	137

investigated materials for LPG gas detection, as shown in Table 3. This table clearly demonstrates that the material ($MoTe_2$) used in this study exhibits a rapid response time (8 s) and excellent recovery time (22 s) at room temperature compared to other materials for LPG sensing. It is interesting to note that the present investigation is carried out at room temperature, whereas others are reported at higher temperature. Furthermore, it is also clear from Table 3 that the present work has a much better response time (8 s) than the other materials reported at room temperature for the detection of LPG. Therefore, the $MoTe_2$ nanomaterial is competitive and superior to many of the reported materials that often require elevated operating temperatures or exhibit slower dynamics. This demonstrates the potential of $MoTe_2$ as a

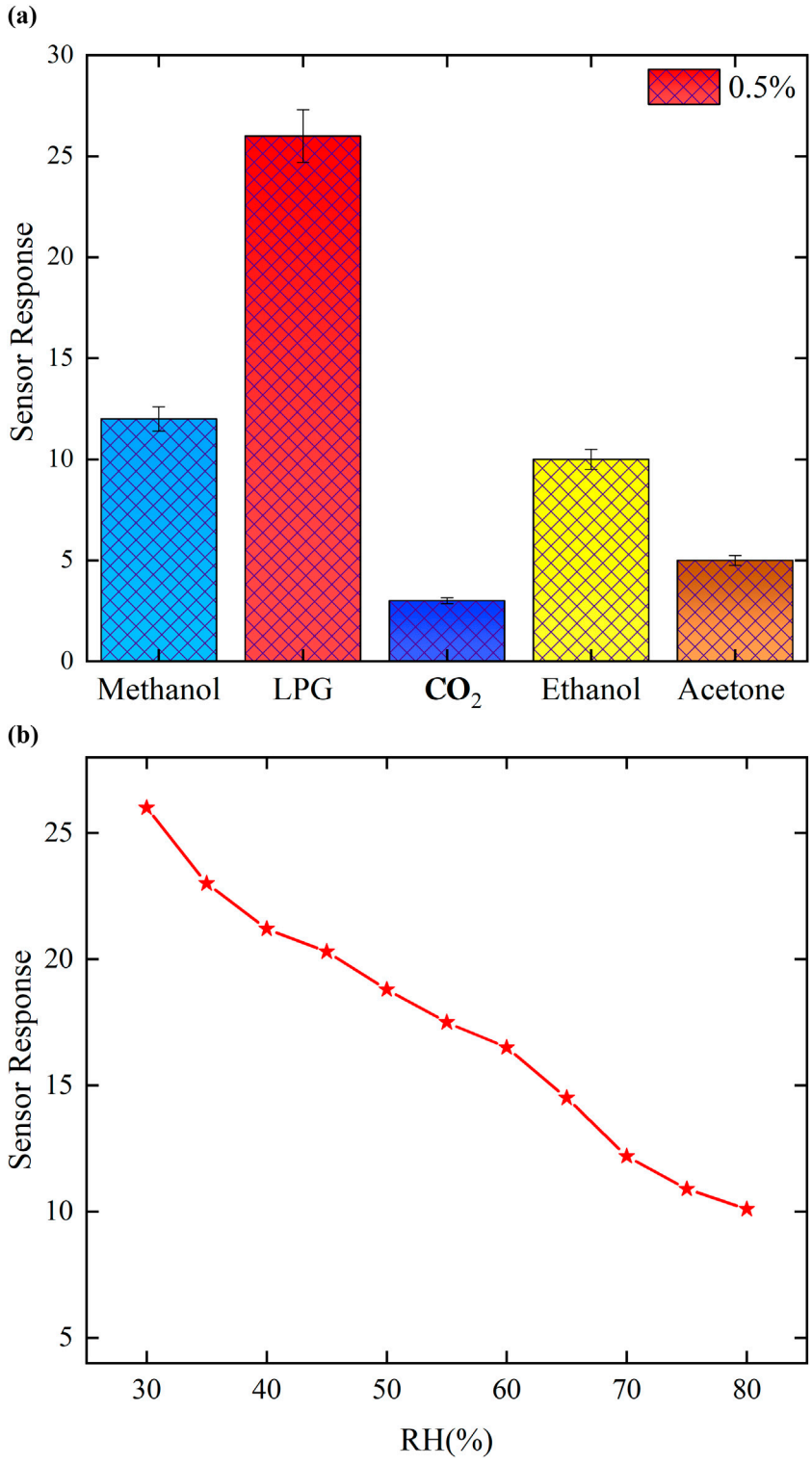

FIGURE 10
(a) Selectivity of the $MoTe_2$ sensor for different target gases at 0.5 vol%. **(b)** Effect of humidity on LPG sensing.

promising material for future development of low-power, high-performance gas sensors operating at room temperature.

The influence of humidity on the sensing performance of $MoTe_2$ thin films has also examined in the presence of 0.5 vol% LPG. The humidity within the chamber increases to 30%–100% using a humidifier with a K_2SO_4-saturated solution, as shown in Figure 10b. In the lower humidity range (30%–45%), the sensor exhibits a strong response, whereas in the mid-range (50%–65%), only minor fluctuations are detected; at elevated humidity levels (70%–90%), the sensor response reduces because at higher humidity,

TABLE 3 Gas-sensing performance of various materials with varying concentrations of LPG.

Material used in sensor fabrication	LPG concentration	Sensor response	Response time	Recovery time	Temperature	Reference
MoS_2/graphene	1,000 ppm	12.2	15 s	22 s	RT	Munusami et al. (2022)
CNT–$LaFeO_3$	250 ppm	480	38 s	347 s	25°C	Yadav et al. (2025)
MWCNT/TiO_2	2.0%	429	36 s	20 s	27°C	Kumar et al. (2024)
rGO–TiO_2	0.5 vol%	136	23 s	20 s	RT	Chaurasiya et al. (2023)
Fe_2O_3:ZnO	2000 ppm	4.8	26 s	15 s	200°C	Aleksanyan et al. (2024)
Ce-ZnO/PANI	100 ppm	79.67	157 s	154 s	RT	Selvakumar et al. (2023)
Ag–CuO:SnO_2	0.5%	300%	21 s	30 s	RT	Verma et al. (2024)
La-substituted Mg–Zn ferrites	500 ppm	36	80 s	156 s	250°C	Mishra et al. (2024)
Fe_3O_4 and ZnO	1,000 ppm	0.96 and 0.84	50 s	70 s	230°C	Kavi et al. (2024)
NiO and Co_3O_4	1,000 ppm	0.8 and 0.79	60 s	60 s	250°C	
$Pr_{0.8}Bi_{0.2}FeO_3$	0.5%	1.2	16.2 s	22.4 s	30°C	Bharati et al. (2024)
ZnO	50 ppm	367	10 s	7 s	350°C	Shinde et al. (2024)
α-Fe_2O_3	90	50	52 s	107 s	170°C	Choudhary et al. (2021)
Mono-metallic Ag NPs	-	2.81	16 s	64 s	RT	Singh and Kumar (2024)
Pd–WO_3	100 ppm	125	8.3 s	27.8 s	175°C	Younes et al. (2022)
$MoTe_2$	0.5%	26	8 s	22 s	RT	This work

physisorption is saturated, and contact between the sensing film and LPG molecules is weaker, resulting in a reduced sensing performance. The $MoTe_2$ thin film is very appropriate for the mid-humidity spectrum.

5 Gas-sensing mechanism

The mechanism of the gas sensing of the $MoTe_2$ sensor shows fluctuation of the charge carrier on thin film surface upon encountering LPG. Thin film surfaces have adsorbed ambient oxygen via charge transfer. Both the molecular (O_2^-) and atomic oxygen (O^- and O^{2-}) species are ionized as surface oxygen. The existence of negative oxygen species is essential for LPG absorption as it has an affinity for O_2^-, which enhances receptor activation. The processes governing oxygen absorption on thin-film surfaces are presented in Equations 5–7:

$$O_{2\,(\text{atmospheric})} \rightarrow O_{2\,(\text{adsorbed}),} \tag{5}$$

$$O_{2\,(\text{adsorbed})} + e^- \rightarrow O^-_{2\,(\text{adsorbed})}, \tag{6}$$

$$O^-_{2\,(\text{adsorbed})} + e^- \rightarrow 2O^-_{(\text{adsorbed}).} \tag{7}$$

In a LPG-containing environment, LPG adsorbed on the thin film's surface interacts through pre-ionized oxygen species and forms hydrogen bonds with the surface molecules and produces changes in electrical resistance. The interaction of LPG and the adsorbed oxygen species is described using chemical reactions outlined in Equations 8 and 9, which illustrate the possible mechanisms underlying the LPG-sensing response. When LPG interacts with chemisorbed oxygen species, a dehydration process occurs, resulting in an unstable intermediate complex (C_nH_{2n}:O) and release of CO_2 and H_2O. The probable reactions are as follows:

$$C_nH_{2n+2} + 2O^- \rightarrow H_2O + C_nH_{2n}\text{: O} + \text{electron}, \tag{8}$$

$$C_nH_{2n}\text{: O} + O^- \rightarrow CO_2 + H_2O + \text{electron}. \tag{9}$$

Here, n is equal to 3 and 4.

On the surface of the thin film, as the concentration of LPG increases, the interaction between LPG and chemisorbed oxygen species also increases. Increased LPG content leads to higher interaction between LPG and chemisorbed oxygen species, resulting in the release of electrons (Equations 8, 9). These electrons then recombine with holes in the p-type material, leading to a reduction in hole concentration. This reduction in majority carriers increases the resistance of the $MoTe_2$ film. The released electron creates a diffusion pathway by reducing the space charge region, facilitating better interaction between gas molecules and the sensor film, which enhances the sensor's performance.

As the LPG concentration increases, the interaction between LPG and chemisorbed oxygen species also increases. As elaborated in Equations 8, 9, the release of electrons increases the height and width of the barrier potential. At saturation, resistance remains

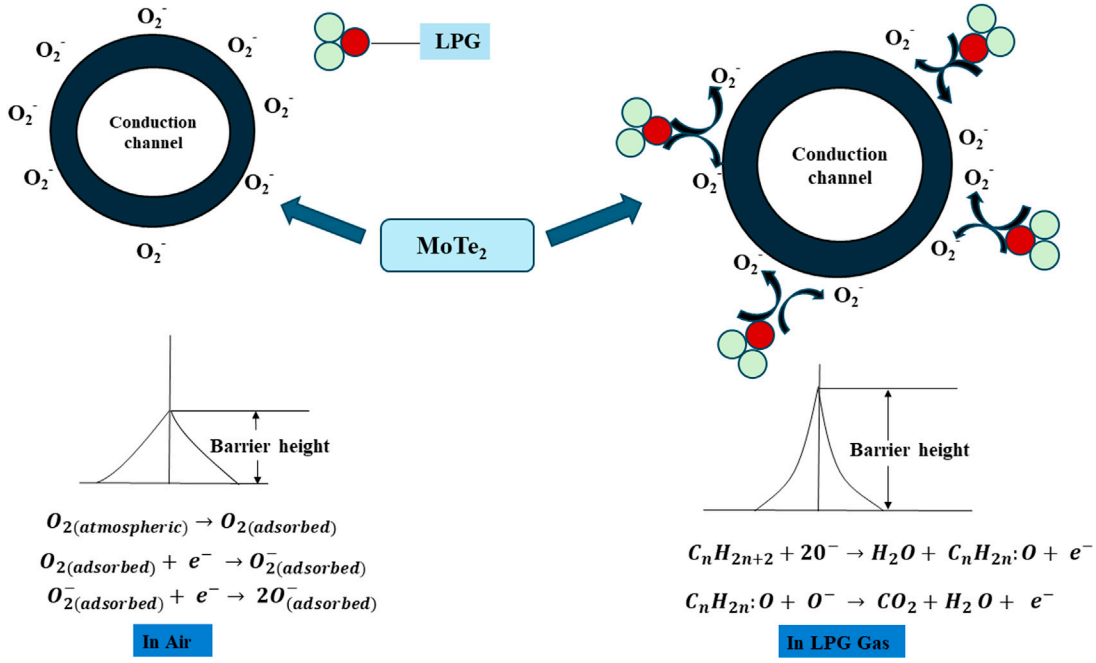

FIGURE 11
Gas-sensing mechanism of $MoTe_2$ thin-film LPG sensing.

constant, and the decrease in resistance upon LPG removal is due to the recovery of surface-adsorbed oxygen species, which re-establish the charge transfer equilibrium and restore hole-rich conditions in the p-type $MoTe_2$ material. The mechanism is schematically depicted in Figure 11. In this study, the $MoTe_2$ thin film serves as an efficient room-temperature LPG sensor capable of detecting trace amounts of LPG with rapid response and fast recovery while exhibiting remarkably high sensor responsivity and sensitivity.

6 Conclusion

In conclusion, a simple and easy hydrothermal method was used for successful synthesis of the $MoTe_2$ nano-materials. The PXRD analysis confirmed the existence of the $MoTe_2$ hexagonal phase, with an average crystallite size of 37.14 nm and percentage crystallinity of 95%. Microstructural, morphological, and elemental analyses of the synthesized $MoTe_2$ revealed thin, wrinkled sheets with a crumpled topology and flake-like structures, along with the presence of Mo and Te elements. Finally, the $MoTe_2$ thin-film sensor was fabricated and tested for room-temperature LPG detection from LPG concentration of 0.5–2.0 vol%. The fabricated sensor demonstrated excellent sensing capabilities with very quick time of response as 8 s and fast time of recovery as 22 s at 0.5 vol% of LPG. The sensitivity of the sensor was found to be 77 sensor responses per concentration. The linear concentration dependence of the sensor's response was found for LPG, with a maximum value of 137 at 2.0 vol% of LPG. The repeatability test was carried out for 1.5 vol% LPG using the $MoTe_2$ thin film, in which four consecutive cycles were performed, and the fabricated sensor showed a repeatability of 99.40% with an error of 0.6%. The fabricated sensing film shows excellent selectivity toward LPG measurements with various analyte gases, such as methanol, LPG, ethanol, acetone, and CO_2, at a concentration of 0.5 vol% and at room temperature. The sensor responses to methanol, LPG, ethanol, acetone, and CO_2 were found to be 12, 26, 10, 5, and 3, respectively. These results indicate that the $MoTe_2$-sensing film exhibits the highest sensitivity to LPG of all other gases. As the findings provide shorter response times and greater LPG sensitivity, this cost-effective synthesized $MoTe_2$ with elongated nano-needle and sheet-like structures shows excellent performance in LPG detection. These features establish $MoTe_2$ as a promising candidate for the next generation of low-power, miniaturized gas sensors, with potential extension to other volatile organic compounds, smart home safety systems, and industrial leak detection networks, and it has the potential to boost the sensing market.

Data availability statement

The original contributions presented in the study are included in the article/Supplementary Material; further inquiries can be directed to the corresponding author.

Author contributions

AS: Investigation, Methodology, Writing – original draft, Formal Analysis, Visualization. AK: Visualization, Investigation, Formal analysis, Writing – review and editing. NC: Writing – review and editing, Visualization, Resources, Validation. AR: Resources, Data curation, Validation, Writing – review and editing. MG: Resources, Data curation, Writing – review and editing, Validation. BY: Resources, Validation, Writing – review and editing. MS: Resources, Formal Analysis, Project administration, Funding acquisition,

Methodology, Supervision, Conceptualization, Writing – review and editing.

Funding

The author(s) declare that no financial support was received for the research and/or publication of this article.

Conflict of interest

The authors declare that the research was conducted in the absence of any commercial or financial relationships that could be construed as a potential conflict of interest.

Generative AI statement

The author(s) declare that no Generative AI was used in the creation of this manuscript.

Publisher's note

References

Abdullah, M., Khan, S., Jabbour, K., Imran, M., Faheem, M., John, P., et al. (2023). Electrochimica acta development of binder-free $MoTe_2$/RGO electrode via hydrothermal route for supercapacitor application. *Electrochimica Acta* 466, 143020. doi:10.1016/j.electacta.2023.143020

Aleksanyan, M., Sayunts, A., Shahkhatuni, G., Shahnazaryan, G., Simonyan, Z., and Kananov, D. (2024). Fabrication of the Fe2O3:ZnO based nanostructured sensor for LPG detection. *E-Journal Surf. Sci. Nanotechnol.* 22 (2), 149–156. doi:10.1380/EJSSNT.2024-008

Bharati, K., Tiwari, P. R., Singh, R. P., Singh, A., Yadav, B. C., Singh, M. P., et al. (2024). Synthesis of bismuth-doped praseodymium ortho ferrite nanomaterials for LPG sensing. *Appl. Nanosci.* 14 (2), 277–289. doi:10.1007/s13204-023-02976-2

Bhat, K. S., and Nagaraja, H. S. (2019). Performance evaluation of molybdenum dichalcogenide (MoX2; X= S, Se, te) nanostructures for hydrogen evolution reaction. *Int. J. Hydrogen Energy* 44 (33), 17878–17886. doi:10.1016/j.ijhydene.2019.05.179

Cao, W., Zhao, Q., Yang, L., and Cui, H. (2021). Enhanced NOx adsorption and sensing properties of MoTe2 monolayer by Ni-Doping: a first-principles study. *Surfaces Interfaces* 26, 101372. doi:10.1016/j.surfin.2021.101372

Chaurasiya, N., Singh, A., Kumar, K., Yadav, B. C., Yadawa, P. K., Singh, S. K., et al. (2023). A highly sensitive room temperature liquefied petroleum gas (LPG) sensor with fast response based on a titanium dioxide (TiO2)-Reduced graphene oxide (r-GO) composite. *Sensors Diagnostics* 2 (5), 1215–1227. doi:10.1039/d2sd00223j

Chen, F., Zhang, Y., Wang, D., Wang, T., Zhang, J., and Zhang, D. (2022). High performance ammonia gas sensor based on electrospinned Co3O4 nanofibers decorated with hydrothermally synthesized MoTe2 nanoparticles. *J. Alloys Compd.* 923, 166355. doi:10.1016/j.jallcom.2022.166355

Choudhary, S., Annapoorni, S., and Malik, R. (2021). Facile strategy to synthesize donut-shaped α-Fe2O3 nanoparticles for enhanced LPG detection. *Sensors Actuators, B Chem.* 334, 129668. doi:10.1016/j.snb.2021.129668

Dai, J., Li, M., and Zeng, X. C. (2016). Group IVB transition metal trichalcogenides: a new class of 2D layered materials beyond graphene. *Wiley Interdiscip. Rev. Comput. Mol. Sci.* 6 (2), 211–222. doi:10.1002/wcms.1243

Feng, Z., Xie, Y., Chen, J., Yu, Y., Zheng, S., Zhang, R., et al. (2017a). Highly sensitive MoTe2 chemical sensor with fast recovery rate through gate biasing. *2D Mater.* 4 (2), 025018. doi:10.1088/2053-1583/aa57fe

Feng, Z., Xie, Y., Wu, E., Yu, Y., Zheng, S., Zhang, R., et al. (2017b). Enhanced sensitivity of MoTe2 chemical sensor through light illumination. *Micromachines* 8 (5), 155. doi:10.3390/mi8050155

Gautam, Y. K., Sharma, K., Tyagi, S., Ambedkar, A. K., Chaudhary, M., and Pal Singh, B. (2021). Nanostructured metal oxide semiconductor-based sensors for greenhouse gas detection: progress and challenges. *R. Soc. Open Sci.* 8 (3), rsos.201324. doi:10.1098/rsos.201324

Grzeszczyk, M., Gołasa, K., Zinkiewicz, M., Nogajewski, K., Molas, M. R., Potemski, M., et al. (2016). Raman scattering of few-layers MoTe2. *2D Mater.* 3 (2), 025010. doi:10.1088/2053-1583/3/2/025010

Guo, H., Yang, T., Yamamoto, M., Zhou, L., Ishikawa, R., Ueno, K., et al. (2015). Double resonance raman modes in monolayer and few-layer MoTe2. *Phys. Rev. B - Condens. Matter Mater. Phys.* 91 (20), 205415–205418. doi:10.1103/PhysRevB.91.205415

Hu, N., Wang, Y., Chai, J., Gao, R., Yang, Z., Kong, E. S. W., et al. (2012). Gas sensor based on P-Phenylenediamine reduced graphene oxide. *Sensors Actuators, B Chem.* 163 (1), 107–114. doi:10.1016/j.snb.2012.01.016

Huang, B., Sun, S., Li, X., Li, X., Wang, N., and Li, X. (2025). Layered MoTe2/ZnO heterojunctions for sensitive TEA sensors at room temperature. *Sensors Actuators B Chem.* 439, 137862. doi:10.1016/j.snb.2025.137862

Island, J. O., Molina-Mendoza, A. J., Barawi, M., Biele, R., Flores, E., Clamagirand, J. M., et al. (2017). Electronics and optoelectronics of Quasi-1D layered transition metal trichalcogenides. *2D Mater.* 4 (2), 022003. doi:10.1088/2053-1583/aa6ca6

Kavi, S. S., Susithra, V., El-Rehim, A. F. A., and Kumar, E. R. (2024). Natural grape juice assisted synthesis of metal oxide nanoparticles: evaluation of microstructural, vibrational and colloidal stability analysis for liquified petroleum gas (LPG) sensor applications. *Sensors Actuators B Chem.* 406, 135451. doi:10.1016/j.snb.2024.135451

Kodan, S., Kumar, A., Sanger, A., Arora, A., Malik, V. K., and Chandra, R. (2024). Vertically aligned MoSe2-WS2 nanoworms heterojunction towards room temperature NO2 gas sensors. *Sensors Actuators B Chem.* 407, 135481. doi:10.1016/j.snb.2024.135481

Kumar, U., Yadav, B. C., Kumar, K., Haldar, T., Kanth Kumar, V. V. R., Huang, W. M., et al. (2024). Exploring the room temperature chemiresistive LPG and humidity sensing properties of MWCNT/TiO2 nanocomposite with DFT interpretations. *Sensors Actuators A Phys.* 379, 115851. doi:10.1016/j.sna.2024.115851

Liu, Y., Shi, T., Si, Q., and Liu, T. (2021). Adsorption and sensing performances of transition metal (Pd, Pt, Ag and Au) doped MoTe2 monolayer upon NO2: a DFT study. *Phys. Lett. Sect. A General, Atomic Solid State Phys.* 391 (2), 127117. doi:10.1016/j.physleta.2020.127117

Liu, Z., Gui, Y., Xu, L., and Chen, X. (2022). Adsorption and gas-sensing properties of aun (n = 1–3) cluster doped MoTe2 for NH3, NO2, and SO2 gas molecules. *Surfaces Interfaces* 30, 101883. doi:10.1016/j.surfin.2022.101883

Lv, Y. Y., Cao, L., Li, X., Zhang, B. B., Wang, K., Pang, B., et al. (2017). Composition and temperature-dependent phase transition in miscible Mo1-x Wx Te2 single crystals. *Sci. Rep.* 7, 44587. doi:10.1038/srep44587

Mishra, B., Nanda, J., Brahma, S. S., Sankaran, K. J., Sakthivel, R., Ghadei, S., et al. (2024). Effect of La3+ doping on structural, magnetic and LPG gas-sensing properties of Mg-Zn nano-ferrites. *Mater. Sci. Eng. B* 299, 117029. doi:10.1016/j.mseb.2023.117029

Munusami, V., Arutselvan, K., Vadivel, S., and Govindasamy, S. (2022). High sensitivity LPG and H2 gas sensing behavior of MoS2/Graphene hybrid sensors prepared by facile hydrothermal method. *Ceram. Int.* 48 (19), 29322–29331. doi:10.1016/j.ceramint.2022.05.334

Octon, T. J., Nagareddy, V. K., Russo, S., Craciun, M. F., and Wright, C. D. (2016). Fast high-responsivity few-layer MoTe2 photodetectors. *Adv. Opt. Mater.* 4 (11), 1750–1754. doi:10.1002/adom.201600290

Panigrahi, P., Hussain, T., Karton, A., and Ahuja, R. (2019). Elemental substitution of two-dimensional transition metal dichalcogenides (MoSe2 and MoTe2): implications for enhanced gas sensing. *ACS Sensors* 4 (10), 2646–2653. doi:10.1021/acssensors.9b01044

Selvakumar, D., Sonu, K. P., Ramadoss, G., Sivaramakrishnan, R., Jayavel, R., Eswaramoorthy, M., et al. (2023). Heterostructures of polyaniline and Ce–ZnO nanomaterial coated flexible PET thin films for LPG gas sensing at standard environment. *Chemosphere* 314, 137492. doi:10.1016/j.chemosphere.2022.137492

Shackery, I., Pezeshki, A., Park, J. Y., Palanivel, U., Kwon, H. J., Yoon, H. S., et al. (2018). Few-layered α-MoTe2 schottky junction for a high sensitivity chemical-vapour sensor. *J. Mater. Chem. C* 6 (40), 10714–10722. doi:10.1039/c8tc02635a

Shinde, P. V., Mane, P., Late, D. J., Chakraborty, B., and Rout, C. S. (2021). Promising 2D/2D $MoTe_2/Ti_3C_2T_x$ hybrid materials for boosted hydrogen evolution reaction. *ACS Appl. Energy Mater.* 4 (10), 11886–11897. doi:10.1021/acsaem.1c02914

Shinde, S., Shinde, V., and Wadkar, P. (2024). Rapid response and quick recovery LPG sensor fabricated using aqueous Sol–Gel synthesized ZnO/Zn(OH)2 hexagonal nanoparticles. *J. Electron. Mater.* 53 (9), 5222–5237. doi:10.1007/s11664-024-11150-5

Shirpay, A., and Mohagheghi, M. M. B. (2020). Investigation of structural, optical and thermoelectric properties of 2H–MoTe2 and MoO3–TeO2 thin films. *Phys. B Condens. Matter* 587, 412141. doi:10.1016/j.physb.2020.412141

Singh, A., Sikarwar, S., and Yadav, B. C. (2021). Design and fabrication of quick responsive and highly sensitive LPG sensor using ZnO/SnO2 heterostructured film. *Mater. Res. Express* 8 (4), 045013. doi:10.1088/2053-1591/abf52e

Singh, M. P., Dhumal, N. R., Kim, H. J., Kiefer, J., and Anderson, J. A. (2017). Removal of confined ionic liquid from a metal organic framework by extraction with molecular solvents. *J. Phys. Chem. C* 121 (19), 10577–10586. doi:10.1021/acs.jpcc.7b02289

Singh, S., and Kumar, G. (2024). Ultra-sensitive liquefied petroleum gas (LPG) sensor based on monometallic Ag nanospheres synthesized *via* microwave-assisted facile approach. *Hybrid. Adv.* 7, 100313. doi:10.1016/j.hybadv.2024.100313

Su, J., Liu, K., Wang, F., Jin, B., Guo, Y., Liu, G., et al. (2019). Van Der Waals 2D Transition Metal Tellurides. *Adv. Mater. Interfaces* 6 (19), 1–17. doi:10.1002/admi.201900741

Szary, M. J., Florjan, D. M., and Bąbelek, J. A. (2022). Selective detection of carbon monoxide on P-Block doped monolayers of MoTe2. *ACS Sensors* 7 (1), 272–285. doi:10.1021/acssensors.1c02246

Tiwari, P. R., Singh, R. P., Bharati, K., Yadav, A. C., Kumar, K., Yadav, B. C., et al. (2022). Magnesium-substituted zinc ferrite as a promising nanomaterial for the development of humidity sensors. *Phys. Status Solidi (A) Appl. Mater. Sci.* 219 (23), 2200424. doi:10.1002/pssa.202200424

Tiwari, P. R., Singh, R. P., Bharati, K., Yadav, A. C., Yadav, B. C., Singh, A., et al. (2024). Synthesis of calcium doped zinc ferrite nanomaterial and its application as a humidity sensor. *J. Dispersion Sci. Technol.* 45 (11), 2155–2165. doi:10.1080/01932691.2023.2256383

Varghese, S. S., Varghese, S. H., Swaminathan, S., Singh, K. K., and Mittal, V. (2015). Two-dimensional materials for sensing: Graphene and beyond. *Electron. Switz.* 4 (3), 651–687. doi:10.3390/electronics4030651

Verma, V., Pandey, N. K., Singh, A., Singh, P., Gupta, P., and Yadav, B. C. (2022). Liquefied petroleum gas (LPG) sensing of biphasic Cu6Sn5:SnO2 nanocomposite thin-films. *Mater. Chem. Phys.* 289, 126459. doi:10.1016/j.matchemphys.2022.126459

Verma, V., Pandey, N. K., Singh, A., Singh, P., Srivastava, S., Yadav, N., et al. (2024). Room temperature LPG sensing of highly responsive Ag-Doped CuO: SnO2 nanocomposite film. *Phys. E Low-Dimensional Syst. Nanostructures* 163, 116035. doi:10.1016/j.physe.2024.116035

Wu, E., Xie, Y., Yuan, B., Hao, D., An, C., Zhang, H., et al. (2018a). Specific and highly sensitive detection of ketone compounds based on P-Type MoTe 2 under ultraviolet illumination. *ACS Appl. Mater. Interfaces* 10 (41), 35664–35669. doi:10.1021/acsami.8b14142

Wu, E., Xie, Y., Yuan, B., Zhang, H., Hu, X., Liu, J., et al. (2018b). Ultrasensitive and fully reversible NO2 gas sensing based on P-Type MoTe2 under ultraviolet illumination. *ACS Sensors* 3 (9), 1719–1726. doi:10.1021/acssensors.8b00461

Wu, Y., Xu, L., and Gui, Y. (2025). Adsorption properties of ZnO-Modified MoTe2 monolayers on H2, CO2, C2H6 gases. *Phys. B Condens. Matter* 714, 417463. doi:10.1016/j.physb.2025.417463

Xu, J., Zhang, J., Zhang, W., and Lee, C. S. (2017). Interlayer nanoarchitectonics of two-dimensional transition-metal dichalcogenides nanosheets for energy storage and conversion applications. *Adv. Energy Mater.* 7 (23), 1–30. doi:10.1002/aenm.201700571

Yadav, A. K., Kumar, U., and Yadav, B. C. (2025). Sol–Gel-processed CNT-doped LaFeO3 and its application as LPG sensor. *J. Mater. Sci. Mater. Electron.* 36 (1), 54–17. doi:10.1007/s10854-024-13931-4

Yan, J., Wang, Y., Yang, C., Deng, H., and Hu, N. (2024). MoS2/MoO3 heterojunctions enabled by surface oxidization of MoS2 nanosheets for high-performance room-temperature NO2 gas sensing. *J. Alloys Compd.* 976, 173208. doi:10.1016/j.jallcom.2023.173208

Younes, N., Kashyout, A. E. H. B., Shoueir, K., and El-Kemary, M. (2022). Palladium doped tungsten oxide nanoparticle nanocomposite for sensitive detection of CO2 and LPG gases. *J. Mater. Res. Technol.* 19, 2633–2644. doi:10.1016/j.jmrt.2022.05.189

Zappa, D. (2017). Molybdenum dichalcogenides for environmental chemical sensing. *Materials* 10 (12), 1418–1422. doi:10.3390/ma10121418

Zhou, L., Xu, K., Zubair, A., Liao, A. D., Fang, W., Ouyang, F., et al. (2015). Large-area synthesis of high-quality uniform few-layer MoTe2. *J. Am. Chem. Soc.* 137 (37), 11892–11895. doi:10.1021/jacs.5b07452

Zhu, H., Cui, H., He, D., Cui, Z., and Wang, X. (2020). Rh-Doped MoTe2 monolayer as a promising candidate for sensing and scavenging SF6 decomposed species: a DFT study. *Nanoscale Res. Lett.* 15 (1), 129. doi:10.1186/s11671-020-03361-6

Zhu, X. F., Wang, L., and Chen, L. F. (2014). Adsorption and dissociation of O2 on MoSe2 and MoTe2 monolayers: Ab *initio* study. *Int. J. Mod. Phys. B* 28 (28), 1450195–11. doi:10.1142/S0217979214501951